Folding of maltose binding protein outside of and in GroEL

Xiang Ye[a], Leland Mayne[a], Zhong-yuan Kan[a], and S. Walter Englander[a,1]

[a]Johnson Research Foundation, Department of Biochemistry and Biophysics, Perelman School of Medicine, University of Pennsylvania, Philadelphia, PA 19104

We used hydrogen exchange–mass spectrometry (HX MS) and fluorescence to compare the folding of maltose binding protein (MBP) in free solution and in the GroEL/ES cavity. Upon refolding, MBP initially collapses into a dynamic molten globule-like ensemble, then forms an obligatory on-pathway native-like folding intermediate (1.2 seconds) that brings together sequentially remote segments and then folds globally after a long delay (30 seconds). A single valine to glycine mutation imposes a definable folding defect, slows early intermediate formation by 20-fold, and therefore subsequent global folding by approximately twofold. Simple encapsulation within GroEL repairs the folding defect and reestablishes fast folding, with or without ATP-driven cycling. Further examination exposes the structural mechanism. The early folding intermediate is stabilized by an organized cluster of 24 hydrophobic side chains. The cluster preexists in the collapsed ensemble before the H-bond formation seen by HX MS. The V9G mutation slows folding by disrupting the preintermediate cluster. GroEL restores wild-type folding rates by restabilizing the preintermediate, perhaps by a nonspecific equilibrium compression effect within its tightly confining central cavity. These results reveal an active GroEL function other than previously proposed mechanisms, suggesting that GroEL possesses different functionalities that are able to relieve different folding problems. The discovery of the preintermediate, its mutational destabilization, and its restoration by GroEL encapsulation was made possible by the measurement of a previously unexpected type of low-level HX protection, apparently not dependent on H-bonding, that may be characteristic of proteins in confined spaces.

GroEL | protein folding | HX MS

The GroEL chaperonin captures incompletely folded proteins at specific sites on its apical domains and displaces them into the GroEL central cavity where they can fold in isolation protected from aggregation. After ATP hydrolysis (2–10 s), the GroES lid dissociates and releases the substrate protein, either fully folded or not, in which case it may rebind and recycle (1–5). Many chaperone proteins function simply to bind and maintain incompletely folded proteins and thus avoid aggregation or promote other functions such as cross-membrane transport (6, 7). The complex GroEL molecular machine (8) has been thought to play more active roles (9–18), but this view is controversial (19–21). Possible mechanisms include forceful unfolding to reverse misfolding errors (9–11), promotion of conformational searching by limiting the volume of search space (13), and a role for special properties of the GroEL cavity and its walls (12, 22, 23).

Difficulties of measurement have limited these studies. One generally does not even know the structural problem that GroEL may act to resolve. Accordingly, most experiments on GroEL function simply ask about the overall folding rate and yield of a given substrate protein, which reveals neither the specific protein folding problem nor the GroEL repair mechanism (although see refs. 14, 24, and 25). It has been difficult to define protein folding mechanisms, either with or without chaperonin assistance, because intermediates on the pathway between unfolded and native states only live for a very short time and cannot be isolated and studied by the usual structural methods.

We used a hydrogen exchange pulse-labeling mass spectrometry method (HX MS) (26–28) that is uniquely able to define the details of protein folding intermediates and pathways, both with

and without GroEL intervention. We studied the folding of wild-type (WT) maltose binding protein (MBP^{WT}; with the leader sequence removed) and a mutated version (MBP^{V9G}) that imposes a definable folding defect. (Residue numbering for the plasmid construct used here is the canonical numbering +1.) The HX MS method is able to provide time- and sequence-resolved information on MBP in the collapsed ensemble, and on its folding when in free solution, and when it is in the GroEL cavity under passive confinement or active ATP-turnover conditions.

The results confirm (29) yet another case of an obligatory on-pathway folding intermediate, consistent with the foldon-dependent defined pathway model (30–32) but not with the funneled landscape many-pathway model (33). They uncover, in the prefolding collapsed ensemble, a previously unknown organized precursor of the initial on-pathway H-bonded intermediate. When the precursor is disrupted by a destabilizing mutation, folding of the initial intermediate is greatly slowed. Simple GroEL encapsulation restabilizes the precursor and restores fast folding, even without ATP and substrate cycling.

Results

The HX MS Folding Experiment. When denaturant-unfolded *Escherichia coli* MBP is diluted into folding conditions not complicated by aggregation (21) (concentration 1 μM, unfolding by acid urea, no Cl$^-$, pH 7.4, 22 °C; more details in *SI Appendix*), it rapidly collapses (<40 ms) into a dynamic polyglobular ensemble and then more slowly folds to its native state (29). The course of folding was probed by exposure to a brief high D$_2$O acidity (pD) H-to-D HX-labeling pulse. This strategy labels, in a structure-sensitive way, folding intermediates that are present at any time during folding as the protein moves to its native state. Amide sites in segments that are not yet

---

Significance

The GroEL/ES chaperonin is known to prevent protein aggregation during folding by passive containment within the central cavity. The possible role of more active intervention is controversial. The HX MS method documents an organized hydrophobically stabilized folding preintermediate in the collapsed ensemble of maltose binding protein. A mutational defect destabilizes the preintermediate and greatly slows folding of the subsequent on-pathway H-bonded intermediate. GroEL encapsulation alone, without ATP and substrate protein cycling, restabilizes the preintermediate and restores fast folding. The mechanism appears to depend on forceful compression during confinement. More generally, these results suggest that GroEL can repair different folding defects in different ways.

protected by H-bond formation at the time of the D-labeling pulse become fully deuterated (heavier) while sites that are already folded and protected remain undeuterated (lighter). To resolve the positions of the HX-labeled sites, samples were quenched (pH 2.4, 0 °C) to halt further exchange and injected into an online flow-analysis system (*SI Appendix*, Fig. S1). The flow system proteolytically fragments the protein, then separates and analyzes the resulting peptides, roughly by reverse-phase liquid chromatography and then at high-resolution by MS.

MS/MS analysis identified 519 peptide fragments, including 375 unique peptides (*SI Appendix*, Fig. S2). We chose 92 that redundantly cover the entire length of the 370-residue MBP protein and could always be measured with high quality when analyzed by the ExMS program (27). Examination of the many H/D-labeled peptides reveals the identity of folding intermediates and the folding rate, sequence of formation, stability, and dynamic properties of the protein segments that they represent. The comparison of many overlapping peptides provides increased structural resolution and internal consistency checks. HX MS experiments were supplemented by the observation of global MBP folding kinetics by intrinsic tryptophan fluorescence with and without ATP turnover.

Spontaneous Folding of MBP^{WT}. Fig. 1 illustrates pulse-labeling HX MS data for the folding of a peptide (22–44) that covers one segment of an initial MBP folding intermediate and another peptide (170–193) that monitors a segment that folds much later. The bimodal isotopic MS envelopes indicate that, during folding, each segment switches from an unfolded unprotected condition (heavier) to folded and protected (lighter) in a concerted reaction,

as has been found for other proteins (30–32). At each folding time point, the fraction of the protein population that has already folded any particular segment can be read out as the fraction of the lighter (protected) peptide isotopic envelope. The measurement has high accuracy because all of the necessary information, the relative envelope areas, is wholly contained in each bimodal MS trace.

Pulse-labeling data for many peptides placed within the early intermediate, the blue curves in Fig. 1, trace its time-dependent folding. In MBP^{WT}, the half-time for formation of the early intermediate in free solution is 1.2 s (Fig. 1*A*; 1.0–1.5 s total range among the various peptides). The protein segments that form the H-bonded intermediate structure, residues 22–44 and 264–279, are remote in the amino acid sequence but they are in direct contact in the native protein and fold at identical rates, implying that they come together into a relatively native-like configuration, as has been seen for folding intermediates in other proteins (31, 32). The nearly identical behavior of many overlapping peptides provides multiple consistency checks. The difference in folding rate compared with a previous report (29) is due to the different conditions used (7 s half-time at pD 9 vs. 1.2 s at pH 7.4 used here).

The rest of the protein encounters a large kinetic barrier and folds much more slowly. Unlike the tightly determined time course for the many peptides that show formation of the early intermediate, the slow-folding segments that track later global folding are spread over some width on the time axis, with half-times of 20–40 s, suggesting more than one folding step. The suggestive groupings indicated in color represent sets of protein segments that are adjacent in the native protein (*SI Appendix*, Fig. S3). Sequential multistep folding pathways have been seen for other proteins (31, 32). However, in the present case, a large
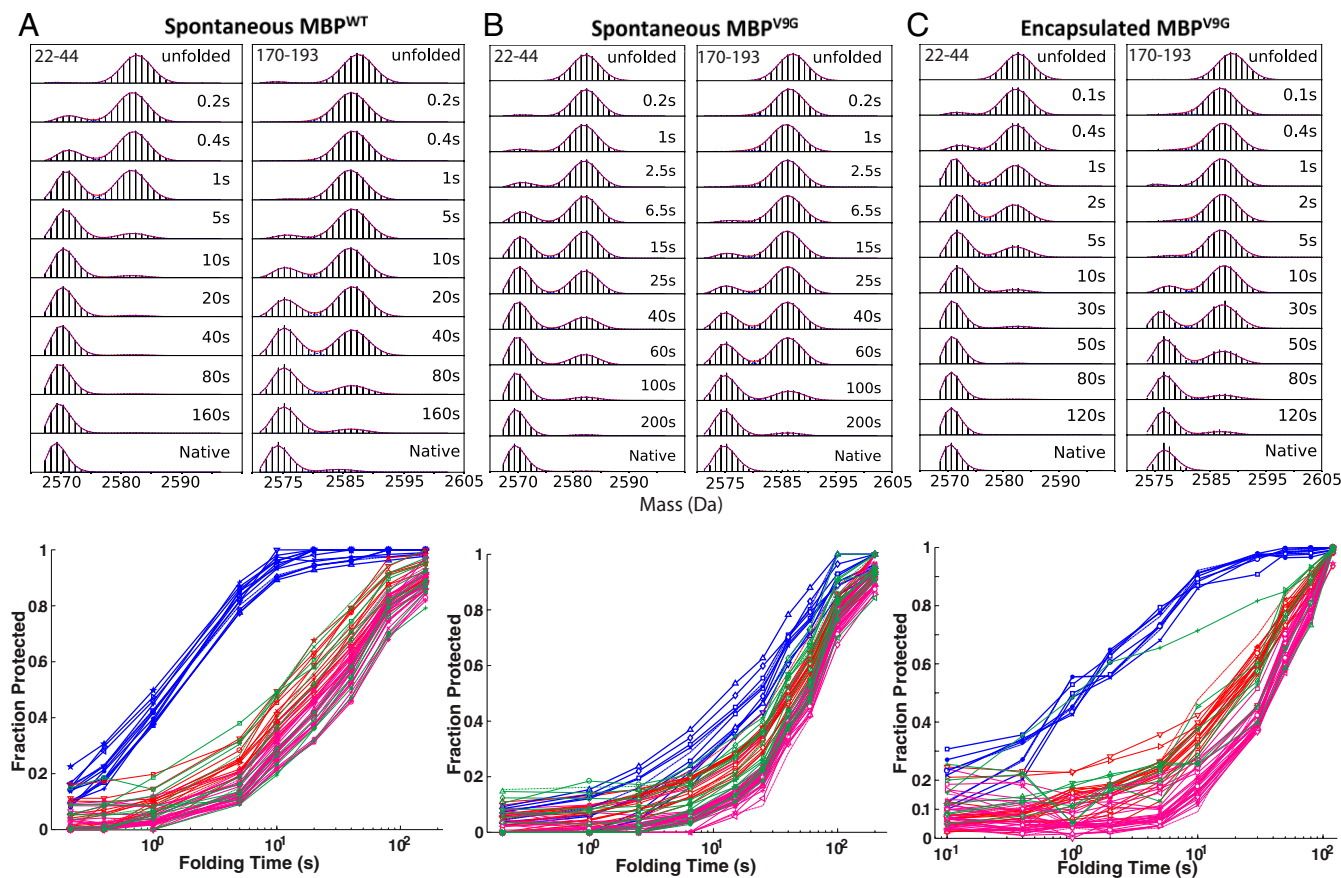
Fig. 1. MBP folding. *Upper* panels show the time-dependent folding of two MBP segments observed by HX MS H-to-D pulse labeling (20-ms pulse). One segment (22–44) participates in the MBP early folding intermediate (~1 s half-time), the other (170–193) folds much later (~40 s). (*A*) The WT protein in free solution (collapsed ensemble). (*B*) The V9G mutated variant (MBP^{V9G}) in free solution. (*C*) MBP^{V9G} encapsulated in GroEL^{D398A}. *Lower* panels track the folding of the early intermediate (blue) and global folding (multicolor), measured by many peptides.
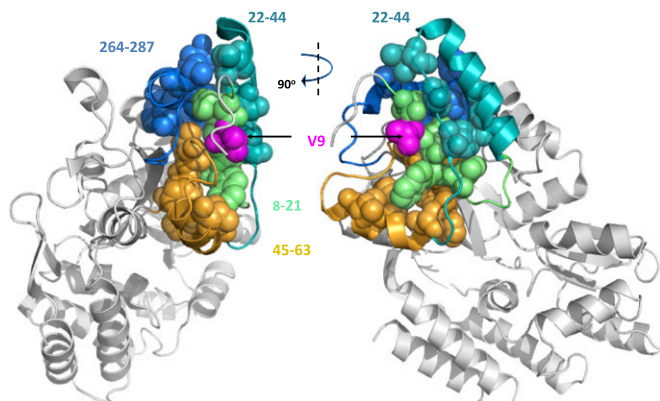
Fig. 2. The preintermediate hydrophobic cluster. The extensive hydrophobic side-chain interactions that stabilize the preintermediate in the initial collapsed ensemble are shown in space-filling representation as they are seen in the native protein. They are as follows: L8, V9, I10, W11, I12, L21, V24, F28, I34, V36, V38, L44, F48, V51, I60, I61, F62, W63, L276, F280, L281, Y284, L285, and L286.

kinetic barrier after formation of the early intermediate is essentially rate-limiting, which makes the separation of later steps ambiguous.

Examination of the cognate structure of the early folding intermediate in the native protein shows that it is stabilized, in part, by a system of 24 hydrophobically interacting side chains, shown in space-filling representation in Fig. 2. The hydrophobic cluster contains the protein segments just noted, the sequentially distant sequences 22–44 and 264–279, which form the H-bonded HX-protected early folding intermediate, and also the neighboring 9–21 and 45–60 segments which fold later. Six amino acid substitutions are known to slow MBP folding (34, 35); all are placed within the segments pictured. These segments all exhibit weak protection against HX labeling in the initial collapsed ensemble, well before the later formation of the strongly protected H-bonded intermediate just described. Many other segments also exhibit weak protection in the collapsed ensemble. However, unlike the other peptides, the segments pictured in Fig. 2, some near and some far in the sequence, are all destabilized by a single mutation at sequence position Val9 (see below). These several observations consistently indicate that some approximation to this structure preexists as a preintermediate in the collapsed ensemble.

Spontaneous Folding of MBP^{V9G}. We prepared MBP with the substitution Val9Gly (MBP^{V9G}) placed within the cluster in Fig. 2. When MBP^{V9G} is in free solution, the early intermediate folds more slowly, by 20-fold with a half-time of ∼25 s (Fig. 1B). As expected for an obligatory on-pathway intermediate, they remain the first elements to fold (blue segments in Fig. 1B). Because subsequent steps are much slower, global folding is delayed by about the same absolute amount, making it slower by approximately twofold.

The same HX MS methods were used to observe the folding of MBP^{V9G} when it is inside the GroEL/ES cavity (Fig. 1C). In these experiments, a modification of the online analysis system was used to remove GroEL and GroES before the MBP proteolysis step to avoid overwhelming the MS analysis with many peptide fragments (*SI Appendix*, Fig. S1). The additional time needed in the online peptide analysis (10 min) adds trivially to D-back exchange during the analysis (*SI Appendix*, Fig. S4).

Encapsulation restores the fast folding rate of the early intermediate. Average measured half-time is 1.1 s (0.9–1.3 s total range) compared with 1.2 s for folding of MBP^{WT} in free solution. This result is not masked by the time (∼1 s) required to ensure initial encapsulation (10, 36). The course of folding is followed for much longer times (Fig. 1). To ensure that MBP^{V9G} remains in the cavity and folds only therein during the experiment, we used a mutant GroEL, D398A, which hydrolyzes ATP so slowly (∼30 min half-time) (37–39) that ATP turnover and substrate protein cycling do not occur during the folding experiment. ATP binding triggers substrate protein

encapsulation with GroES capping, and folding occurs in the static cavity (Fig. 1C) without substrate protein cycling. The results therefore measure the effect of static encapsulation alone.

The Role of Substrate Cycling. To directly compare the effect of encapsulation with and without substrate cycling, we employed intrinsic MBP^{V9G} fluorescence (Fig. 3). These experiments compare the global folding of MBP^{V9G} in GroEL^{WT} with ATP-dependent substrate cycling to folding in GroEL^{D398A} without cycling. (GroEL/ES has no tryptophan and no interfering fluorescence.) In both cases, global folding of MBP^{V9G} returns to the rate found for MBP^{WT} in free solution. ATP-dependent substrate cycling does not produce faster folding than static encapsulation alone. Fig. 3 also shows the absence of any folding when MBP^{V9G} is bound to the GroEL apical domains before encapsulation.

The approximately twofold acceleration of MBP^{V9G} global folding, which might otherwise be thought to represent a direct GroEL effect, is fully accounted for as an indirect effect of the recovered fast formation of the prior on-pathway intermediate. Encapsulation itself, with or without ATP-dependent cycling, has no effect on the large kinetic barrier that limits the MBP global folding rate. Similarly misleading behavior can be expected for any other case that ignores pathway intermediates and focuses only on the effect of GroEL on the final global folding step.

The Collapsed Ensemble. To understand the GroEL mechanism, we pursued a more thorough analysis of MBP folding. Protein folding studies often detect a fast initial collapse of an unfolded protein into a molten globule type of ensemble before folding. Much attention has been directed to the condition of structure and stability in the collapsed ensemble, its possible role in guiding subsequent native-state formation, and the relationship with various physical measurements [FRET, small-angle X-ray diffraction, circular dichroism (CD)] (40, 41).

In previous work, HX protection has been connected to specific amide hydrogen bonding in native secondary structures (42, 43) and commonly exhibits protection factors in the range of Pf ∼10^3 and far higher. These numbers indicate free energy of stabilization over 4 kcal/mol [protection factor (Pf) = HX = HX reference rate for fully unprotected amides (44)/measured HX rate]. We report here HX MS observations on the structure and dynamic properties of MBP in the collapsed ensemble where many peptides display a much lower level of HX protection.
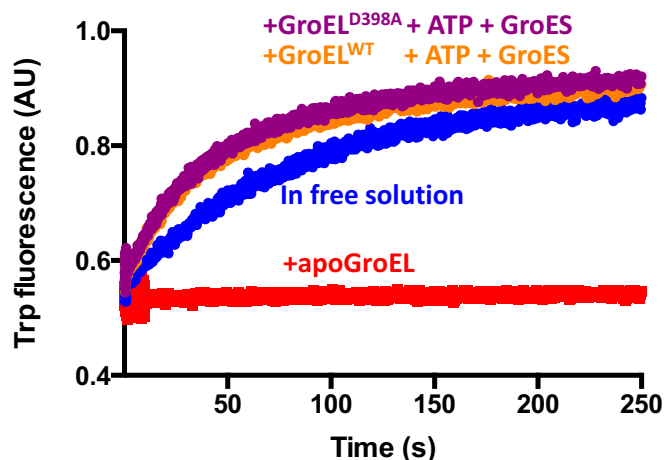
Fig. 3. Global folding by fluorescence. The global folding of mutant MBP^{V9G} followed by the intensity of intrinsic tryptophan fluorescence when free in solution (blue), when bound to the GroEL apical domains (red), and in the GroEL cavity with ATP-dependent cycling (in WT GroEL; orange) and without cycling (in mutant D398A GroEL; purple). GroEL/ES has no tryptophan and therefore no interfering fluorescence. (Excitation at 295 nm, observation through a 305-nm long-pass filter, Biologic SFM400 stopped flow; Grenoble.) AU, arbitrary units.

To assess weak HX protection, unfolded MBP^{WT} was diluted into folding conditions to populate the collapsed ensemble and then exposed to increasingly long 10- to 80-ms H-to-D labeling pulses. Representative peptides are shown in Fig. 4. The segment 22–44 is a part of the fast intermediate. In the 0.2-s delay before the labeling pulse, ~10% have already formed the well-protected intermediate (left envelope), as expected ($t_{1/2}$ = 1.2 s). The major not-yet-folded population fraction (unprotected, heavy) can be separately observed. Some amides exchange within the weakest 10-ms pulse (Pf < 5). A few sites are more resistant but become labeled by longer pulses, emphasized by the blue and red vertical dashed lines, which serves to quantify their low-level protection (Pf < 50, stabilization free energy <2 kcal/mol). Many other peptides, like 45–62 and 179–196, also show low-level protection in the collapsed ensemble. A few, like 293–302, have little or no residual protection.

Peptides in four sequence regions (90–114, 150–160, 240–265, 341–351) show broadened or clearly bimodal HX EX1 isotopic envelopes (*SI Appendix*, Fig. S5). EX1 kinetics measures cooperative segmental unfolding reactions, suggesting α-helical secondary structure due to burial in the collapsed state (45). The EX1 peptides do have high hydrophobic content, but other segments that have high hydrophobicity do not show EX1 behavior (*SI Appendix*, Fig. S6). They seem likely to produce CD and other spectroscopic signals in the collapsed ensemble, although they are mainly in β-sheet conformation in the native MBP protein. Even the apparently structured EX1 segments show only weak stability; the EX1 folded to unfolded ratio extrapolated to zero pulse-labeling length (K = 1) indicates a stabilization free energy close to zero. Interestingly, encapsulation often slows the EX1 unfolding rate as well as other EX2 HX rates (*SI Appendix*, Fig. S5B). Also interesting is the fact that these EX1 peptides, with some structure in the unfolded state, do not contribute to the early intermediate.

Preintermediate in the Collapsed Ensemble. The V9G mutation has no effect on measurable HX in the collapsed ensemble, with one notable exception. It selectively abolishes the weak residual HX protection of the hydrophobic cluster segments that will become strongly protected in the early intermediate (22–44, 264–279) (Fig. 5B). Other peptides that monitor these same protein segments confirm the effect. Cluster segments that will fold much later (9–21, 45–62) are partially but not completely destabilized (*SI Appendix*, Fig. S7). All other peptides are wholly unaffected.

This observation requires that, well before the formation of the HX-protected intermediate (1.2 s; Fig. 1A), the hydrophobic cluster segments, although distant from each other in sequence, are already spatially grouped together immediately adjacent to the Val9 position. The preintermediate cluster appears to be held together by the cooperative more or less native-like interaction of its many hydrophobic side chains (Fig. 2), even before it clicks into its more strictly correct format enforced by the more demanding H-bond constraints observed by strong HX protection.

The Role of Encapsulation. In Fig. 1, the main variable is folding time. Fig. 5 extends those observations by varying pulse strength to measure the weakly stable preintermediate. There is a short delay before the H-to-D labeling pulse is applied, 0.2 s for the collapsed ensemble (Fig. 5 A and B), and 2 s for MBP^{V9G} in GroEL^{D398A} (Fig. 5C; to ensure full encapsulation). During the delay time, some population fraction folds and some does not. The resulting bimodal envelopes separately measure the population fractions already folded and not yet folded. The folded fraction is ~10% of the MBP^{WT} population in A, zero for MBP^{V9G} in B, and over half for encapsulated MBP^{V9G} in C. These results match the folding results in Fig. 1.

The pulse-labeling MS data in Fig. 5 also measure HX protection of the still-unfolded population fraction. These molecules are not affected by the prior folding time (Fig. 1). The hydrophobic cluster peptides are weakly protected in A, destabilized in B, and reprotected in C. The relative stability of the preintermediate is displayed more quantitatively by the line plots in Fig. 5 D and E and in *SI Appendix*, Fig. S7. The curves plot the fractional D-uptake of the not-yet-folded peptides as a function of pulse time. For
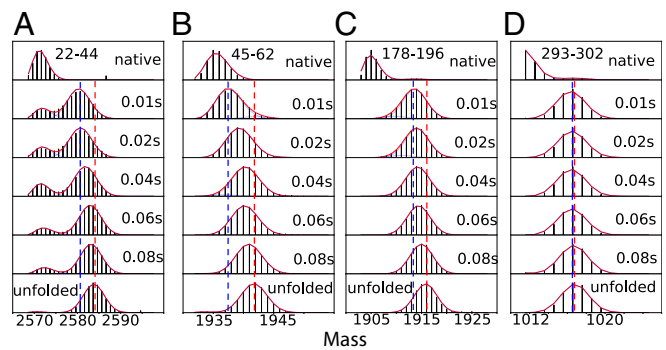
Fig. 4. Low-level HX protection in the collapsed ensemble. Unfolded MBP^{WT} was diluted into folding conditions and brief H-to-D labeling pulses of increasing length were applied (10–80 ms at pD 9.8, 22 °C where intrinsic free peptide half-time is 0.5–5 ms). Weak HX protection is seen for hydrophobic cluster peptides, like 22–44 (A), which forms the early H-bonded intermediate (~10% folding has already occurred), and for 45–62 (B), which does not, and also for many noncluster peptides (C) but not for some others (D). Vertical lines are added to aid visualization of increasing deuteration with longer but still weak labeling pulses. Other peptides with EX1 character are shown in *SI Appendix*, Fig. S5.

each noted peptide, these curves compare the amount of D-labeling found for MBP^{WT} in free solution (blue; from panel A), for MBP^{V9G} in free solution (red; from panel B), and when MBP^{V9G} is statically encapsulated in the GroEL^{D398A} cavity (orange; from panel C). In the collapsed ensemble of MBP^{WT} in free solution, the cluster segments show their characteristic weak protection (blue), and they fold rapidly. They are selectively destabilized by the V9G substitution (red) and then fold more slowly. Restabilization upon encapsulation (orange) restores their fast folding.

A noncluster peptide is also shown (Fig. 5F), typical of many others that display weak protection in the collapsed ensemble. Their red and blue curves are identical because they are not destabilized by the V9G mutation. Like the cluster peptides, encapsulation stabilizes them (less D-labeling). Unlike the cluster peptides, their folding rate is not affected by encapsulation. Thus, the stabilization seen for the mutant preintermediate is due to a general nonselective encapsulation-dependent effect.

In these experiments, the preintermediate was identified by virtue of the selective destabilization of the hydrophobic cluster peptides by the V9G mutation. The placement of the mutation was guided by knowledge of the early on-pathway MBP folding intermediate (Fig. 2). Does the weak protection seen for many other peptides in the collapsed ensemble reflect similar native-like association or simply random hydrophobic association? Some more general mutational scanning together with appropriate HX methods might help to illuminate this interesting question.

Discussion

Protein Folding Mechanism. Experiments have found a dozen proteins that fold through native-like foldon-dependent intermediates in defined pathways (30–32). The present results confirm (29) that MBP is one of these. Additional results extend the defined intermediate view. A distinct weakly stabilized precursor preexists in the initially collapsed MBP ensemble, held together apparently by a relatively native-like cluster of interacting hydrophobic side chains. The generality of this behavior remains to be tested.

GroEL Mechanism. Another result of the present work is that GroEL can greatly accelerate the formation of the early on-pathway MBP folding intermediate when its folding is impaired. A deeper insight is that GroEL accomplishes this function not by acting on the intermediate itself but, in the case of MBP, on a precursor form. Enclosure in the GroEL cavity exercises a widespread nonspecific effect that suppresses segmental dynamics throughout the substrate protein and promotes stability against HX labeling. The same effect restabilizes
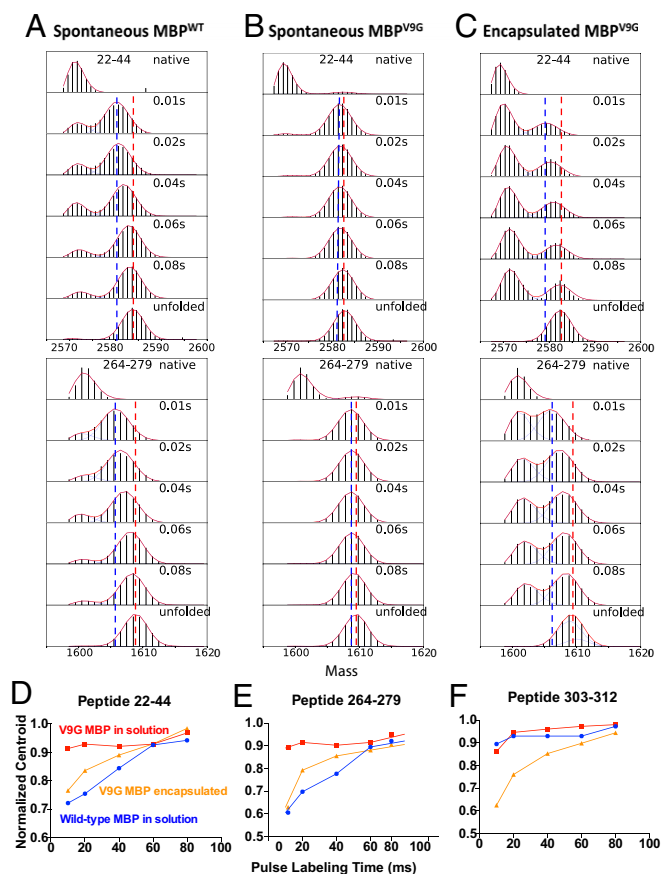
Fig. 5. Intermediate and preintermediate formation. WT and mutant MBP were exposed to H-to-D labeling pulses of increasing length, either in free solution (*A* and *B*) or in the cavity of noncycling GroEL^{D398A} (*C*). (*A*) After 0.2 s of folding (delay time before HX pulse), H-to-D pulse labeling shows that a small fraction of two hydrophobic cluster segments in MBP^{WT} has folded (fast folding rate as expected from Fig 1*A*), and the not-yet-folded fraction has some low-level protection indicating presence of the pre-intermediate. The vertical lines emphasize the response to increasing but still weak labeling pulses. (*B*) The V9G mutation selectively abolishes the low-level stability of the preintermediate peptides and eliminates the fast folding of the early intermediate (as in Fig. 1*B*). (*C*) Encapsulation restores low-level stability in the preintermediate peptides and fast formation of the early intermediate (more folding due to a 2-s delay before the pulse, needed to allow full encapsulation). (*D* and *E*) Line plots summarizing the response—added D labeling—of the hydrophobic cluster peptides to the increasingly long HX-labeling pulse for the following: MBP^{WT} in free solution (blue), MBP^{V9G} in free solution (red), and MBP^{V9G} in GroEL (orange). Normalized centroid means the degree of H-to-D labeling plotted as the fractional D value between the protected native value (lighter) and the unprotected unfolded value. This normalization cancels any effect of a difference in back exchange between different runs. (See *SI Appendix*, Fig. S7 for other cluster peptides.) (*F*) Line plot for a typical noncluster peptide not affected by the V9G mutation but nevertheless endowed with HX protection by encapsulation.

the mutationally impaired MBP^{V9G} hydrophobic cluster and restores its rate for folding to the early intermediate.

These results can be summarized as follows:

$$MBP^{WT}: U \rightarrow CE \rightleftarrows PI \rightarrow I \rightarrow N \qquad [1]$$

$$MBP^{V9G}: U' \rightarrow CE' \rightleftarrows PI' \rightarrow I' \rightarrow N'$$
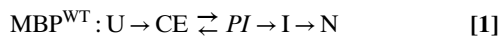
CE is the collapsed ensemble. PI is the hydrophobically stabilized, preintermediate state that is measurable by low-level HX protection.

I is the stably H-bonded early intermediate measured by HX MS in free solution and in the GroEL cavity for both the MBP WT and V9G variants. The prime symbol distinguishes states where the V9G mutation is present, but structures are otherwise equivalent so far as we can tell. However, the CE to PI equilibria are different. In MBP^{WT}, the forward equilibrium, CE to PI, is dominant (PI is measured), and the half-time for then forming I is 1.2 s. In MBP^{V9G} the CE' to PI' equilibrium is disfavored, reducing the rate for forming the H-bonded I by 20-fold. GroEL encapsulation promotes association equilibria in general, which restores the CE to PI equilibrium and the fast I formation rate.

A widely considered possibility is that GroEL encapsulation acts to speed structure formation entropically by promoting the required conformational search. Against this view is the fact that encapsulation broadly suppresses rather than promotes conformational dynamics (e.g., *SI Appendix*, Fig. S5). Also, the deleterious effect of the V9G mutation seems unlikely to work by slowing pre-intermediate formation directly. Formation of the precursor is intrinsically fast, <40 ms. A 1,000-fold slowing due to the mutation seems unlikely. The restoration of fast folding appears to be due to an encapsulation-dependent promotion of the CE to PI equilibrium (Eq. 1), dependent on suppression of the PI dissociation rate, just as EX1 unfolding is suppressed (*SI Appendix*, Fig. S5), and thus may reflect a general function of GroEL confinement.

One possibility is that the encapsulation-dependent mechanism is based on the compression of proteins within the tightly confining cavity. Chen and Makhatadze (46) have shown that pressure stabilizes hydrophobic interactions in water due to an equilibrium PΔV effect. (This is opposite to the destabilization of native proteins by high pressure, which is based on the elimination of voids in structured proteins.) A similar effect due to space-requiring intracavity GroEL oligopeptide tails and charge groups on the GroEL inner wall has been noted before (1, 12, 15, 22). This effect can usefully come into play when folding is limited by the need to form long-range, hydrophobically stabilized segmental interactions.

The compression effect considered here takes its place within a list of other possible strategies, including simple sequestration, forceful unfolding to reverse folding errors (9–11), and wall and oligopeptide tail effects (12, 15, 22). A more general implication is that the GroEL molecular machine may well encompass a variety of mechanisms that can act to repair different kinds of protein folding defects in different ways.

HX Methodology.

A basic problem for folding and chaperone studies is the difficulty of defining the protein folding problem that the chaperone may act to repair and the functional mechanism that it applies to do so. The HX MS method employed here is uniquely able to define structural and dynamical details of protein folding intermediates and pathways during normal and interrupted folding (31, 32). We used these methods to study a designed folding defect, its influence in free solution, and its interaction with GroEL, both with and without active ATP-dependent cycling.

This work uncovered an unusual type of protein HX behavior. All past HX work on protein structural dynamics and function has depended on the ability of HX measurement to distinguish H-bonded structure and its stability. The structural resolving power of that work has profited from the fact that HX slowing of the different amides is usually spread out over many orders of magnitude on the HX time axis. The present results depend on a quality of HX that is different. The incorporation of polypeptide into a viscid molten globule-like ensemble produces a very modest level of HX slowing, with protection factors <50, that seems not to depend on regular H-bonding. This subtle but still measurable property made it possible to recognize the more or less organized hydrophobic cluster preintermediate state of MBP, its concerted destruction by a single mutation, and its recovery upon GroEL encapsulation.

Materials and Methods

The MBP^{WT} plasmid was the same construct as in ref. 47, which has the N-terminal signal peptide removed, a methionine insertion at the N terminus, and an Ile2 to Thr substitution. We use here the sequence numbering for normal

wild-type MBP + 1. Both MBP^{WT} and MBP^{V9G} were overexpressed in *E. coli* and purified from the soluble fraction of the cell extract as described in ref. 29, including rigorous removal of bound maltose. GroEL and GroES were overexpressed and purified according to previous publications (48), including acetone treatment as an additional step to remove contaminating substrate proteins, leaving <10% substrate protein per GroEL heptameric ring, as assessed by tryptophan fluorescence.

HX MS methodology (27, 29) and analysis (49) were described in detail before (26, 28). To avoid interference by many GroE peptides in the HX MS experiments, MBP was quickly separated from GroEL and GroES by a short reverse-phase C4 column inserted into the online flow analysis system and

then diluted 10-fold to reduce CH$_3$CN concentration before flow through the immobilized protease column (*SI Appendix*, Fig. S1). The C4 column has almost no effect on back exchange (*SI Appendix*, Fig. S4). Otherwise, folding in GroEL was studied using the same HX pulse-labeling and analysis methods as before (*SI Appendix, SI Methods*).

1. Hayer-Hartl M, Bracher A, Hartl FU (2016) The GroEL-GroES chaperonin machine: A nano-cage for protein folding. *Trends Biochem Sci* 41:62–76.
2. Taguchi H (2015) Reaction cycle of chaperonin GroEL via symmetric "football" intermediate. *J Mol Biol* 427:2912–2918.
3. Gruber R, Horovitz A (2016) Allosteric mechanisms in chaperonin machines. *Chem Rev* 116:6588–6606.
4. Horwich AL, Fenton WA (2009) Chaperonin-mediated protein folding: Using a central cavity to kinetically assist polypeptide chain folding. *Q Rev Biophys* 42:83–116.
5. Saibil HR, Fenton WA, Clare DK, Horwich AL (2013) Structure and allostery of the chaperonin GroEL. *J Mol Biol* 425:1476–1487.
6. Avellaneda MJ, Koers EJ, Naqvi MM, Tans SJ (2017) The chaperone toolbox at the single-molecule level: From clamping to confining. *Protein Sci* 26:1291–1302.
7. Kim YE, Hipp MS, Bracher A, Hayer-Hartl M, Hartl FU (2013) Molecular chaperone functions in protein folding and proteostasis. *Annu Rev Biochem* 82:323–355.
8. Xu Z, Horwich AL, Sigler PB (1997) The crystal structure of the asymmetric GroEL-GroES-(ADP)7 chaperonin complex. *Nature* 388:741–750.
9. Todd MJ, Lorimer GH, Thirumalai D (1996) Chaperonin-facilitated protein folding: Optimization of rate and yield by an iterative annealing mechanism. *Proc Natl Acad Sci USA* 93:4030–4035.
10. Lin Z, Madan D, Rye HS (2008) GroEL stimulates protein folding through forced unfolding. *Nat Struct Mol Biol* 15:303–311.
11. Shtilerman M, Lorimer GH, Englander SW (1999) Chaperonin function: Folding by forced unfolding. *Science* 284:822–825.
12. Gupta AJ, Haldar S, Miličić G, Hartl FU, Hayer-Hartl M (2014) Active cage mechanism of chaperonin-assisted protein folding demonstrated at single-molecule level. *J Mol Biol* 426:2739–2754.
13. Chakraborty K, et al. (2010) Chaperonin-catalyzed rescue of kinetically trapped states in protein folding. *Cell* 142:112–122.
14. Georgescauld F, et al. (2014) GroEL/ES chaperonin modulates the mechanism and accelerates the rate of TIM-barrel domain folding. *Cell* 157:922–934.
15. Tang YC, et al. (2006) Structural features of the GroEL-GroES nano-cage required for rapid folding of encapsulated protein. *Cell* 125:903–914.
16. Ye X, Lorimer GH (2013) Substrate protein switches GroE chaperonins from asymmetric to symmetric cycling by catalyzing nucleotide exchange. *Proc Natl Acad Sci USA* 110:E4289–E4297.
17. Mattoo RU, Goloubinoff P (2014) Molecular chaperones are nanomachines that catalytically unfold misfolded and alternatively folded proteins. *Cell Mol Life Sci* 71:3311–3325.
18. Fawzi NL, Libich DS, Ying J, Tugarinov V, Clore GM (2014) Characterizing methyl-bearing side chain contacts and dynamics mediating amyloid β protofibril interactions using ^{13}C (methyl)-DEST and lifetime line broadening. *Angew Chem Int Ed Engl* 53:10345–10349.
19. Horwich AL, Apetri AC, Fenton WA (2009) The GroEL/GroES cis cavity as a passive anti-aggregation device. *FEBS Lett* 583:2654–2662.
20. Apetri AC, Horwich AL (2008) Chaperonin chamber accelerates protein folding through passive action of preventing aggregation. *Proc Natl Acad Sci USA* 105:17351–17355.
21. Tyagi NK, Fenton WA, Deniz AA, Horwich AL (2011) Double mutant MBP refolds at same rate in free solution as inside the GroEL/GroES chaperonin chamber when aggregation in free solution is prevented. *FEBS Lett* 585:1969–1972.
22. Weaver J, Rye HS (2014) The C-terminal tails of the bacterial chaperonin GroEL stimulate protein folding by directly altering the conformation of a substrate protein. *J Biol Chem* 289:23219–23232.
23. Sirur A, Knott M, Best RB (2014) Effect of interactions with the chaperonin cavity on protein folding and misfolding. *Phys Chem Chem Phys* 16:6358–6366.
24. Hofmann H, et al. (2010) Single-molecule spectroscopy of protein folding in a chaperonin cage. *Proc Natl Acad Sci USA* 107:11793–11798.
25. Chen DH, et al. (2013) Visualizing GroEL/ES in the act of encapsulating a folding protein. *Cell* 153:1354–1365.
26. Mayne L (2016) Hydrogen exchange mass spectrometry. *Methods Enzymol* 566:335–356.
27. Mayne L, et al. (2011) Many overlapping peptides for protein hydrogen exchange experiments by the fragment separation-mass spectrometry method. *J Am Soc Mass Spectrom* 22:1898–1905.
28. Gallagher ES, Hudgens JW (2016) Mapping protein-ligand interactions with proteolytic-fragmentation, hydrogen/deuterium exchange-mass spectrometry. *Methods Enzymol* 566:357–404.
29. Walters BT, Mayne L, Hinshaw JR, Sosnick TR, Englander SW (2013) Folding of a large protein at high structural resolution. *Proc Natl Acad Sci USA* 110:18898–18903.
30. Englander SW, Mayne L (2017) The case for defined protein folding pathways. *Proc Natl Acad Sci USA* 114:8253–8258.
31. Englander SW, Mayne L, Kan ZY, Hu W (2016) Protein folding-how and why: By hydrogen exchange, fragment separation, and mass spectrometry. *Annu Rev Biophys* 45:135–152.
32. Englander SW, Mayne L (2014) The nature of protein folding pathways. *Proc Natl Acad Sci USA* 111:15873–15880.
33. Onuchic JN, Wolynes PG (2004) Theory of protein folding. *Curr Opin Struct Biol* 14:70–75.
34. Chun SY, Strobel S, Bassford P, Jr, Randall LL (1993) Folding of maltose-binding protein. Evidence for the identity of the rate-determining step in vivo and in vitro. *J Biol Chem* 268:20855–20862.
35. Betton JM, Hofnung M (1996) Folding of a mutant maltose-binding protein of Escherichia coli which forms inclusion bodies. *J Biol Chem* 271:8046–8052.
36. Motojima F, Chaudhry C, Fenton WA, Farr GW, Horwich AL (2004) Substrate polypeptide presents a load on the apical domains of the chaperonin GroEL. *Proc Natl Acad Sci USA* 101:15005–15012.
37. Koike-Takeshita A, Yoshida M, Taguchi H (2008) Revisiting the GroEL-GroES reaction cycle via the symmetric intermediate implied by novel aspects of the GroEL(D398A) mutant. *J Biol Chem* 283:23774–23781.
38. Yang D, Ye X, Lorimer GH (2013) Symmetric GroEL:GroES2 complexes are the protein-folding functional form of the chaperonin nanomachine. *Proc Natl Acad Sci USA* 110:E4298–E4305.
39. Fenton WA, Kashi Y, Furtak K, Horwich AL (1994) Residues in chaperonin GroEL required for polypeptide binding and release. *Nature* 371:614–619.
40. Fuertes G, et al. (2017) Decoupling of size and shape fluctuations in heteropolymeric sequences reconciles discrepancies in SAXS vs. FRET measurements. *Proc Natl Acad Sci USA* 114:E6342–E6351.
41. Aznauryan M, et al. (2016) Comprehensive structural and dynamical view of an unfolded protein from the combination of single-molecule FRET, NMR, and SAXS. *Proc Natl Acad Sci USA* 113:E5389–E5398.
42. Linderstrøm-Lang K (1958) Deuterium exchange and protein structure. *Symposium on Protein Structure*, ed Neuberger A (Methuen, London).
43. Skinner JJ, Lim WK, Bédard S, Black BE, Englander SW (2012) Protein dynamics viewed by hydrogen exchange. *Protein Sci* 21:996–1005.
44. Bai Y, Milne JS, Mayne L, Englander SW (1993) Primary structure effects on peptide group hydrogen exchange. *Proteins* 17:75–86.
45. Dill KA (1985) Theory for the folding and stability of globular proteins. *Biochemistry* 24:1501–1509.
46. Chen CR, Makhatadze GI (2017) Molecular determinant of the effects of hydrostatic pressure on protein folding stability. *Nat Commun* 8:14561.
47. Gardner KH, Zhang XC, Gehring K, Kay LE (1998) Solution NMR studies of a 42 kDa Escherichia coli maltose binding protein beta-cyclodextrin complex: Chemical shift assignments and analysis. *J Am Chem Soc* 120:11738–11748.
48. Grason JP, Gresham JS, Widjaja L, Wehri SC, Lorimer GH (2008) Setting the chaperonin timer: The effects of K$^+$ and substrate protein on ATP hydrolysis. *Proc Natl Acad Sci USA* 105:17334–17338.
49. Kan ZY, Mayne L, Chetty PS, Englander SW (2011) ExMS: Data analysis for HX-MS experiments. *J Am Soc Mass Spectrom* 22:1906–1915.